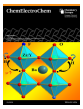

Fluoride-Based Anion Doping: A New Strategy for Improving the Performance of Protonic Ceramic Conductors of the Form $BaZrO_3$

Jun Gao,[a] Yinqiao Liu,[b] Yuqing Meng,[a] Ming Hu,[b] and Kyle S. Brinkman*[a]

A new strategy is reported to improve the performance of $BaZrO_3$-based protonic ceramic conductors by substitution on the anion sublattice, specifically replacing F^- in the O^{2-} site. The F^--doped material exhibited higher conductivity under both reducing and oxidizing atmospheres compared to the undoped oxide. Ab initio calculations and X-ray photoelectron spectroscopy results showed that the improved performance can be attributed to weakened chemical bonding between the cations (A or B site) and the oxygen ions as a result of F^- doping, resulting in improved oxygen mobility. Finally, improved performance was demonstrated by using $BaZr_{0.8}Y_{0.2}O_{3-\delta-\sigma}F_\sigma$ ($\sigma = 0.1$) as the electrolyte in protonic ceramic fuel cells measurements. The anions doping strategy shows great promise for the development of a new generation of high-performance electrolyte materials.

1. Introduction

Solid oxide fuel cells (SOFCs) are promising energy generation systems which have attracted worldwide interest due to their high efficiency, fuel flexibility and low pollution.[1–5] However, the high operating temperature (more than 800 °C) for traditional oxygen ion SOFCs based on the yttrium stabilized zirconia (YSZ) electrolyte limits practical applications. Recently, SOFCs based on protonic conductors called protonic ceramic fuel cells (PCFCs) have attracted significant interest due to the lower operation temperature (below 700 °C) resulting from the lower activation energy for protonic transport as compared to oxygen ion transport in the respective materials systems.[6]

The state of the art electrolyte materials for PCFCs are $BaCeO_3$ and $BaZrO_3$- based materials.[7–10] Doped $BaCeO_3$ shows a higher proton conductivity under humified atmosphere. However, it exhibits low chemical stability under CO_2 and H_2O due to the large Brønsted basicity.[11] Doped $BaZrO_3$ exhibits lower proton conductivity while maintaining good chemical stability under water and carbon dioxide containing atmosphere resulting from its shorter and stronger Zr–O bonds (in comparison with Ce–O) and practically an ideal combination between Zr–O and Ba–O bond distances.[12] A large number of elements were selected as the dopants in $BaZrO_3$ to improve its proton conductivity or transport characteristics such as yttrium, ytterbium, thulium, scandium, holmium and Zinc.[13–17] Among them, yttrium is considered as the most promising dopant. For example. Tong et al. developed a cost-effective solid-state reactive sintering method to fabricate dense $BaZr_{0.8}Y_{0.2}O_{3-\delta}$ (BZY) membranes with high proton conductivity.[18] In addition, Bi et al. successfully fabricated BZY electrolyte films by utilizing the driving force from anode substrate to obtain a dense electrolyte at temperatures near 1400 °C.[19]

To date, the doping strategy has focused on the doping cations in the A or B site. In this work, we report a new route for improving the conductivity of BZY via doping F^- in the anion sublattice at oxygen sites. Fluoride has a higher electronegativity than oxygen, which will lead to the attraction of electrons. As a result, doping F^- into the oxygen sites may reduce the valence electron density of oxygen ions, weaken the chemical bonds between cations and oxygen ions, and lead to faster oxygen mobility in the bulk oxide. The improved oxygen mobility should contribute to the improvement of protonic mobility and conductivity. This strategy has been widely studied in mixed conductors. For example, Zhu et al. reported unprecedented oxygen permeation membrane by doping F^- in $SrCo_{0.9}Nb_{0.1}O_{3-\delta}$.[20] High performance perovskite cathode for SOFCs was developed by Zhang et al. through embedding anions (F^-) in oxygen sites.[21] Also, Chen et al. found the higher hydrogen permeability and better stability hydrogen separation membranes can be achieved by doping Cl^- in $La_{5.5}W_{0.6}Mo_{0.4}O_{11.25}$.[22] This suggests that through anions doping, the properties and performance of a wide range of proton conducting ceramics may be tailored.

However, so far, only a small number of reports have examined the strategy in protonic ceramic condutors. Tarasova et al, found that the mobility of oxygen and proton were improved by doping small amount of F^- in $Ba_2In_2O_5$.[23] Su et al. demonstrated a stable electrolyte by doping F^- in barium cerate oxides.[24] Higher conductivity was observed for the Br^- doped $BaCe_{0.8}Y_{0.2}O_{3-\delta}$ but with poor stability than the parent perovskite.[25]

[a] J. Gao, Dr. Y. Meng, Prof. K. S. Brinkman
Department of Materials Science and Engineering
Clemson University, Clemson, SC, 29634, USA
E-mail: ksbrink@clemson.edu
[b] Dr. Y. Liu, Prof. M. Hu
Department of Mechanical Engineering
University of South Carolina, Columbia, SC 29201

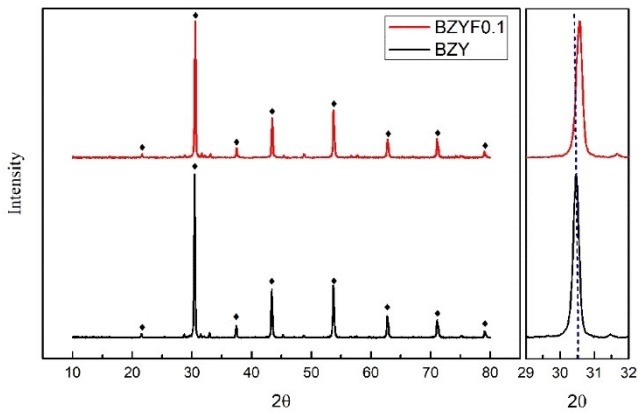

Figure 1. XRD patterns of $BaZr_{0.8}Y_{0.2}O_{3-\delta-\sigma}F_{\sigma}$ ($\sigma = 0$, 0.1) membranes

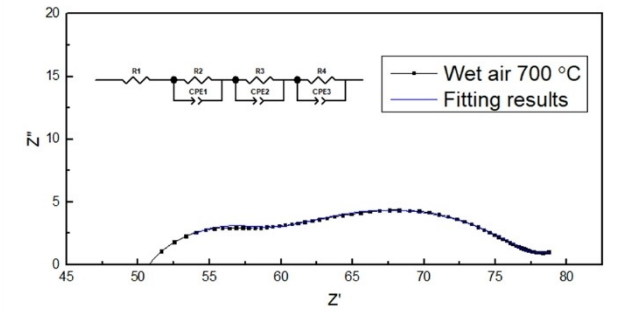

Figure 2. Nyquist plots of $BaZr_{0.8}Y_{0.2}O_{3-\delta-\sigma}F_{\sigma}$ ($\sigma = 0.1$) sample under wet air at 700 °C and the equivalent circuit for fitting the impedance spectra.

In this work, we demonstrated that anion doping can enhance the performance of $BaZrO_3$- based protonic ceramic conductors. F^- was selected as the dopant for O^{2-} site in BZY. We found an enhanced conductivity under both reducing and oxidizing atmospheres, and the improvement was contributed by the increased oxygen mobility in the lattice. The results show that anions doping is a promising way to tailor the properties of $BaZrO_3$- based protonic ceramic conductors which are the compositions of interest for a wide range of energy conversion and storage devices at present.

2. Results and Discussion

Figure 1 displays the X-ray diffraction (XRD) patterns in $BaZr_{0.8}Y_{0.2}O_{3-\delta-\sigma}F_{0.1}$($BZYF_{0.1}$), indicating phase pure perovskite with no BaF_2 secondary phase detected. All samples exhibited a cubic structure, which suggest that F^- were successfully doped into the oxide lattice for $BZYF_{0.1}$. In addition, patterns show that doping F^- induces a shift in diffraction peaks to higher 2-theta, which corresponds to a decrease in the lattice parameter with F^- dopant.

Figure 2 shows a representative Nyquist plot of $BaZr_{0.8}Y_{0.2}O_{3-\delta-\sigma}F_{\sigma}$ ($\sigma = 0.1$) sample impedance spectrum under wet air at 700 °C. The impedance spectrum typically has three semicircles corresponding to the bulk, grain boundary and electrodes responses from high to low frequency, which can be fitted by equivalent circuit model. The insert in Figure 2 is the R-CPE model used to fit the impedance in this work.

Figure 3 displays the Arrhenius plot of the total conductivity of $BaZr_{0.8}Y_{0.2}O_{3-\delta-\sigma}F_{\sigma}$ ($\sigma = 0$, 0.1) as a function of temperature under different atmospheres. The co-substitution of Y^{3+} and F^-

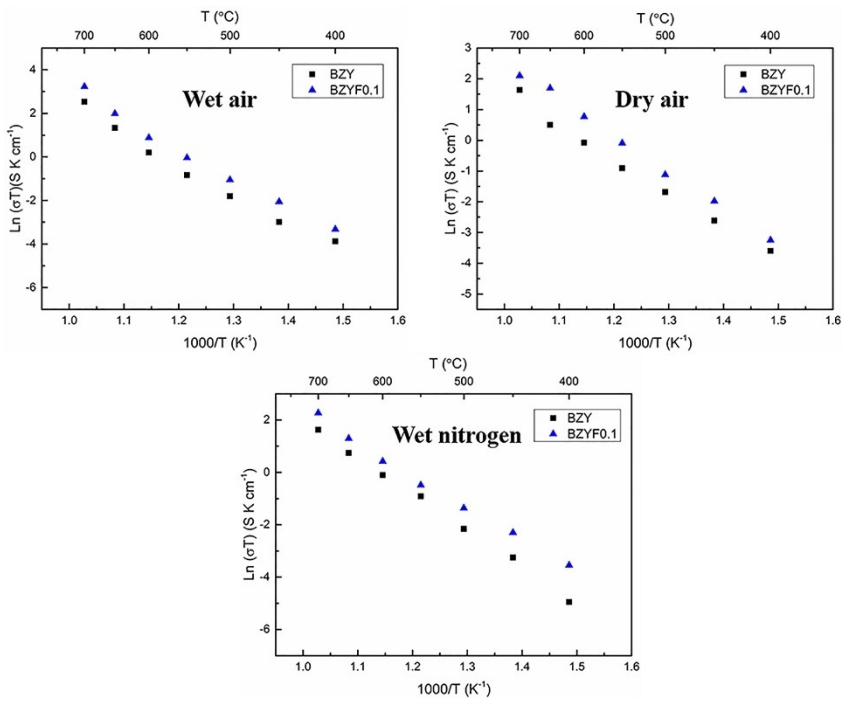

Figure 3. Electrical conductivity of $BaZr_{0.8}Y_{0.2}O_{3-\delta-\sigma}F_{\sigma}$ ($\sigma = 0$, 0.1) under wet air, dry air and wet nitrogen from 700°C to 400°C.

in $BaZrO_3$ oxide can be described as the Eqs. (1)–(3) in Kröger-Vink notation.

$$Y_2O_3 \xrightarrow{B_aZ_rO_3} 2Y'_{Zr} + 3O^X_O + V^{\cdot\cdot}_O \quad (1)$$

$$B_aF_2 \xrightarrow{B_aZ_rO_3} B_{aB_a}^X + 2F_O^{\cdot} + V''_{B_a} \quad (2)$$

$$V''_{B_a} + V^{\cdot\cdot}_O \rightarrow \text{Null} \quad (3)$$

As expected, addition of F^- will reduce the oxygen vacancies in BZY. However, fluoride has a higher electronegativity (4.0) than oxygen (3.44), which allows it to attract electrons more strongly than oxygen. This would result in a decrease in the metal-oxygen bond energy, making oxygen ions easier to be displaced from neighboring cations contributing to the formation of additional oxygen vacancies. Clearly, $BZYF_{0.1}$ has higher conductivity compared to un-doped materials in the different atmospheres examined in this study. In wet nitrogen, the higher total conductivity resulting from the contribution of protons originates from the increased concentration of oxygen vacancies or increased mobility of oxygen lattice, as shown by Eq. (4)

$$H_2O + O^X_O + V^{\cdot\cdot}_O \rightarrow 2OH^{\cdot} \quad (4)$$

Improved oxygen ion and proton conductivity were achieved under dry and wet air after introduction of F^- in the oxygen lattice. The improved proton conductivity is determined by the oxygen vacancy concentration and the mobility of ionic charge carriers in the perovskite.

Oxygen vacancy concentration is one factor that affects the proton conductivity in wet atmosphere. Thermal expansion behavior analysis was used to identify the oxygen vacancies after F^- doping. According to Tor S. Bjørheim's calculation work,[26] there appears to be a correlation between the oxygen vacancy concentration with the linear thermal expansion over a certain temperature range. As shown in Figure 4a, $BZYF_{0.1}$ has a lower thermal expansion than the parent BZY sample from 400 to 1000 K, which indicates that doped F^- in BZY had a decreased oxygen vacancy concentration. This observation was consistent with the calculated thermal expansion coefficient by first-principles density functional theory (DFT). As show in Figure 4b, $BZYF_{0.1}$ has a lower calculated thermal expansion coefficient. This result suggests that the introduction of F^- in the lattice will decrease the oxygen vacancies according to the Kröger-Vink notation. Therefore, the observed improvement in the proton conductivity in F^- doped BZY membranes is not a result of the increased oxygen vacancy concentration. Rather, the increased mobility of oxygen and oxygen defects is likely the main reason for the observed performance enhancement.

To understand the increased oxygen mobility in $BZYF_{0.1}$ membrane, XPS was used to analyze the binding energies of oxygen in $BaZr_{0.8}Y_{0.2}O_{3-\delta-\sigma}F_\sigma$ ($\sigma = 0$, 0.1). The binding energy of the oxygen species absorbed on the surface is often higher than that of the oxygen lattice.[27] Figure 5 displays the XPS results indicating the O 1s binding energy of the lattice oxygen species is 526.88 and 527.46 eV for pristine BZY and doped $BZYF_{0.1}$, respectively. The increased binding energy may result from the difference in electronegativity between F^- and O^{2-}, which will weaken the Coulombic force between A or B-site ions and O^{2-}, indicating an increased activity of the lattice oxygen. Notably, the decreased binding energy for metal ions indicates a lower bond energy for metal and oxygen in the perovskite oxides, thus generating faster oxygen mobility in the bulk material. Apparently, the enhanced proton conductivity under wet nitrogen and air originated from the increased mobility of the oxygen lattice and oxygen defects.

The core level of O1s was calculated and shown on Figure 6. The binding energy increased by 0.1 eV after F^- doping, which is consistent with our XPS results. The difference in the oxygen mobility in perovskite material can account for the improved proton conductivity in $BZYF_{0.1}$. This observation is consistent with current literature regarding anion doping on enhancing the mobility of ionic charge carriers as has been observed in other solid-state material systems such as $Ba_2In_2O_5$.[23]

Chemical stability is another important factor for proton ceramic conductors. The sintered pellets were ground into powders and underwent thermogravimetric analysis (TGA) measurements in air and CO_2, as shown on Figure 7. There was an apparent weight loss around 250°C, resulting from the absorbed water in the samples. The $BZYF_{0.1}$ sample maintained good chemical stability both at air and CO_2 at high temperature

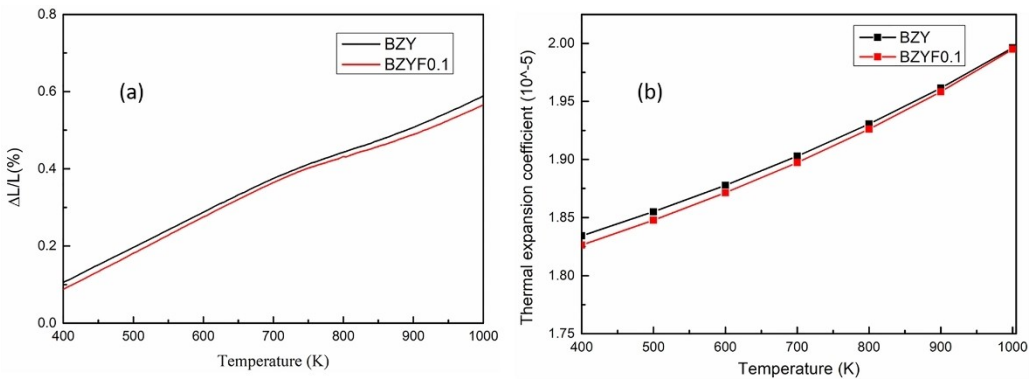

Figure 4. Linear thermal expansion of the $BaZr_{0.8}Y_{0.2}O_{3-\delta-\sigma}F_\sigma$ ($\sigma = 0$, 0.1) samples in air atmosphere (a) and calculated thermal expansion coefficient from DFT calculation (b).

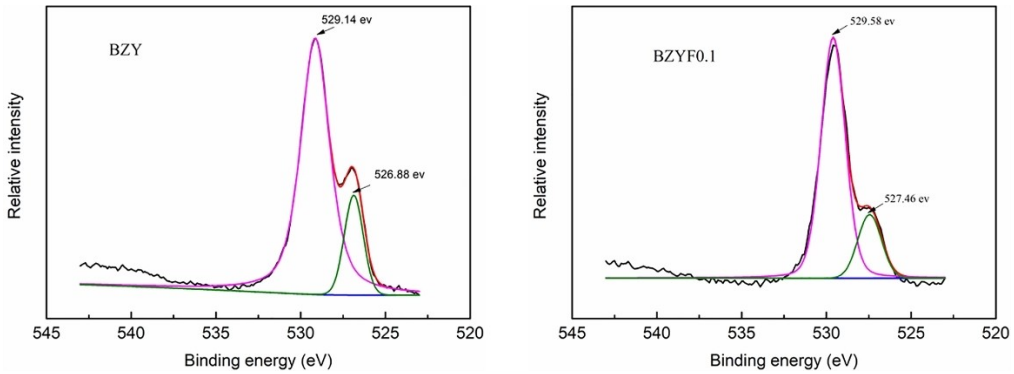

Figure 5. XPS of O 1s peaks for F doped BZY samples.

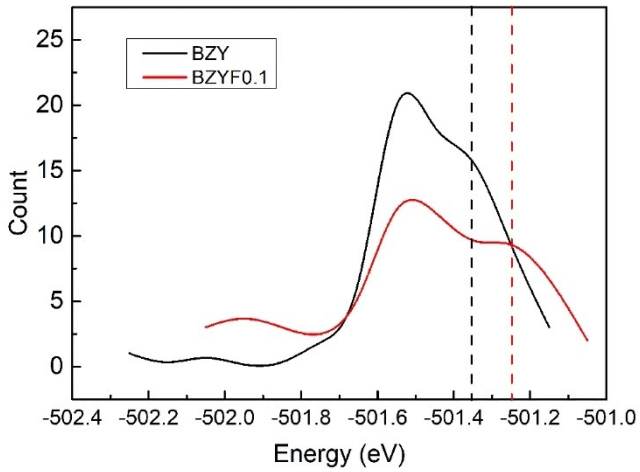

Figure 6. DFT calculation of O1s binding energy in F doped BZY samples.

range, indicating the F^- doping in the perovskite materials does not deteriorate the chemical stability of BZY.

The improved oxygen activity or proton conductivity was further confirmed by investigating the single cells' performance by using BZY and $BZYF_{0.1}$ as electrolyte. Figure 8 shows the SEM micrographs of single cells with $BZYF_{0.1}$ as the electrolyte. The representative porous electrodes with 200 nm grain size exhibited good interfacial connection with the electrolyte and revealed a fine microstructure, no apparent pores were observed in the dense electrolyte (50 μm).

We measured the power density of single cells at temperatures ranging from 550–700 °C. Figure 9 shows the representative performance of single cells with $BZYF_{0.1}$ as the electrolyte at different temperatures. In the EIS plot Figure 9b, single cells with BZY and $BZYF_{0.1}$ as the electrolyte displayed a similar polarization resistance due to the similarity in fabrication process and electrode materials. The only difference observed between the cells was the ohmic resistance resulting from the improved proton conductivity in $BZYF_{0.1}$ attributed to the factors discussed in this manuscript.

3. Conclusions

In conclusion, we have successfully prepared dense oxyfluoride perovskite $BaZr_{0.8}Y_{0.2}O_{3-\delta-\sigma}F_\sigma$ ($\sigma = 0.1$) membranes by a solid-state reaction sintering method. The targeted substitution of F^-, for O^{2-} on the anion sublattice resulted in enhanced proton conductivity originating from the improved oxygen mobility comparing to the parent un-doped oxide. The suggested underlying mechanism is the weakened chemical bonds between cations and oxygen ions in perovskite materials after F^- doping. Finally, improved performance was demonstrated by using $BaZr_{0.8}Y_{0.2}O_{3-\delta-\sigma}F_\sigma$ ($\sigma = 0.1$) as the electrolyte in single cell

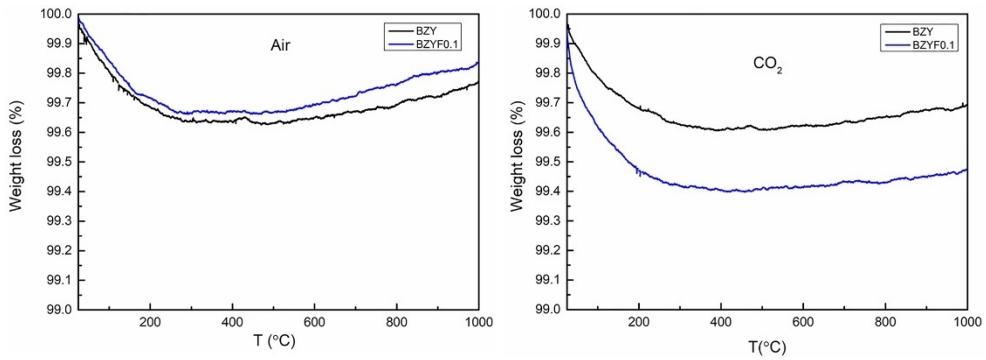

Figure 7. TGA measurements of F doped BZY under air and CO_2 from room temperature to 1000°C.

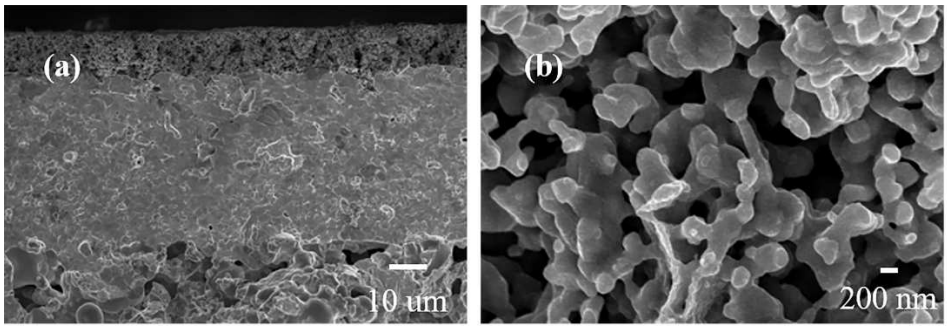

Figure 8. Microstructure of a) NiO-$BZYF_{0.1}$/$BZYF_{0.1}$/PBSCF single cell and b) PBSCF electrode

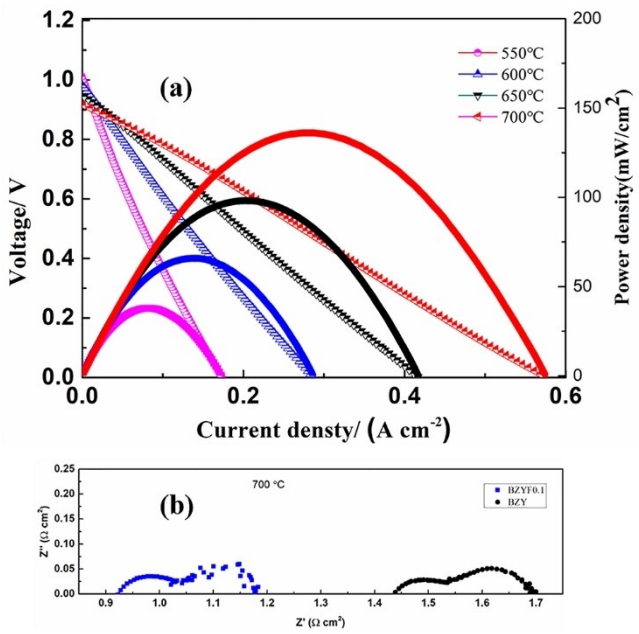

Figure 9. a) Powder density versus current density for single cells with $BZYF_{0.1}$ as the electrolyte and b) Nyquist plots of impedance measured at open circuits with $BZYF_{0.1}$ and BZY as the electrolyte at 700°C.

measurements. The anions doping strategy shows great promise for the development of a new generation of high performance electrolyte materials.

Experimental Section

Powder Synthesis

$PaBa_{0.5}Sr_{0.5}Co_{1.5}Fe_{0.5}O_{5+\delta}$ (PBSCF) was synthesized by a combustion method. 16.346 g $Pr(NO_3)_2$ (Alfa Aesar, 99.99%), 6.534 g $Ba(NO_3)_2$ (Alfa Aesar, 99+%), 5.291 g $Sr(NO_3)_2$ (Alfa Aesar, 98%), 21.828 g Co $(NO_3)_2 \cdot 6H_2O$ (Alfa Aesar, >98.0%) and 10.100 g $Fe(NO_3)_2$ (Alfa Aesar, >98.0%) were dissolved in distilled water, then citric acid (Sigma-Aldrich) and ethylenediaminetetraacetic acid (EDTA, Alfa Aesar) were added to the solution with the metal/citric acid /EDTA ratio of 1:1:1, working as the cheating agent to assist the combustion process. The precursor solution was heated on an oven to form a gel, followed by calcination at 600°C for 4 h to eliminate the organic resides. The calcined power was ball milled in butanol for 24 h and sintered at 1150°C for 12 h to form the pure phase PBSCF.

Membrane Preparation

$BaZr_{0.8}Y_{0.2}O_{3-\delta-\sigma}F_\sigma$ ($\sigma = 0, 0.1$) dense membranes were synthesized by a cost-effective solid-state sintering method.[18] Stoichiometric amounts of $BaCO_3$ (Alfa Aesar, 99.8%), ZrO_2 (Alfa Aesar, 99.7%), Y_2O_3 (Alfa Aesar, 99.9%) and BaF_2 (Alfa Aesar, 99%) with addition of 2.0 wt.% NiO (Alfa Aesar, 99%) as the sintering aid were mixed together in isopropanol with 3-mm yttria-stabilized zirconia (YSZ) beads (Inframat Advanced Materials) for 48 h, followed by drying at 90°C for 24 h. The electrolyte precursor was dry-pressed under 250 MPa for 1 min in a circular carbon-aided steel die with diameter of 15 mm to obtain green electrolyte pellets. The green pellets were sintered at 1500°C for 24 h to obtain dense membranes.

Cell Fabrication

40 wt.% $BaZr_{0.8}Y_{0.2}O_{3-\delta-\sigma}F_\sigma$ ($\sigma = 0, 0.1$) + 60 wt.% NiO anode precursor powder with starch as the pore former were prepared by the same mixing and drying process used for the electrolyte precursor. The anode precursor powder was dry pressed under 250 MPa for 1 min in circular die with the diameter of 15 mm to produce green anode pellets. Electrolyte precursor powder was mixed with binder (5 wt% V-006 (Heraeus) dissolved in terpinol) and dispersant (20 wt% solsperse 28000 dissolved in terpinol) with a ratio of 15:3:1 to form electrolyte slurry that was deposited on each side of the green anode pellets by screen-printing, followed by co-sintering at 1500°C for 24 h. PBSCF slurry was prepared by mixing the PBSCF powder with binder and dispersant. The as-prepared cathode slurry was printed on the electrolyte side and sintered at 950°C for 4 h to obtain single cells.

Calculation Method

First-principles density functional theory (DFT)[28] calculation was performed using the projector augmented wave (PAW) pseudopotential method in conjunction with a plane wave basis set at energy cutoff of 500 eV, as implemented in the Vienna ab initio simulation package (VASP).[29,30] The Perdew-Burke-Ernzerhof (PBE) exchange-correlation functional[31] was used for crystal structure relaxations and formation energies calculations. Monkhorst-Pack-k-points grids of 2×2×2 was used to sample the Brillouin zones for the $BaZr_{0.8}Y_{0.2}O_{3-\delta-\sigma}F_\sigma$ ($\sigma = 0, 0.1$). The theoretical $BaZr_{0.8}Y_{0.2}O_{3-\delta-\sigma}F_\sigma$ ($\sigma = 0, 0.1$) structure was built using a 3×3×3 $BaZrO_3$ supercell with Y, O and F atoms substitution. For example, eliminate 3 O atoms, doping of 6 Y atoms and 8 F atoms result in $Ba_{27}Zr_{21}Y_6O_{70}F_8$, corresponds to a dopant concentration of Y ~ 0.222, F ~ 0.098 and oxygen vacancy

concentration of ~0.111. The thermal expansion was calculated by Gibbs code.[32]

Characterization

The crystalline structure of the samples was characterized using X-ray diffraction (XRD, Rigaku TTR-III diffractometer) with Cu Kα radiation source. The XRD patterns were obtained in the range of 20°–80° with a 0.02° step size and scan speed of 0.5°/min. The microstructure of the dense pellets and single cells were examined using scanning electron microscopy (SEM, Hitachi S-4800). Linear expansion of F^- doped BZY rods were tested by NETZSCH DIL 402 C. The binding energies of O1s in F doped BZY were probed by XPS with an Al Kα X-ray source. The chemical stability of F^- doped BZY under CO_2 and air were detected by TGA using a 7 Pekin Elmer.

Electrochemical Testing

The conductivity of the $BaZr_{0.8}Y_{0.2}O_{3-\delta-\sigma}F_\sigma$ ($\sigma = 0$, 0.1) membranes were tested by electrochemical impedance spectra (EIS), using an electrochemical workstation (Solartron® SI 1287 + 1260) at alternating current (AC) amplitude of 10 mV in the frequency range from 1 MHz to 100 mHz. AC impedance plots were fitted using Zview software according to the equivalent circuit. The performance of single cells was tested with the cathode exposed to dry air and the anode to humified (3% H_2O) hydrogen. Single cells were sealed in an alumina tube by ceramic bond, and silver wires were used as voltage and current leads.

Acknowledgements

The authors gratefully acknowledge the award DE-NE0008703 from the Department of Energy, Nuclear Energy Research Programs (DOE-NEUP) for project CFA-17-12798: Nanostructured Ceramic Membranes for Enhanced Tritium Management.

Conflict of Interest

The authors declare no conflict of interest.

Keywords: protonic ceramic conductor · energy conversion and storage · fluoride ion doping · ab initio calculations · $BaZrO_3$

[1] N. Q. Minh, *J. Am. Ceram. Soc.* **1993**, *76*, 563–588.
[2] Z. Zhan, S. A. Barnett, *Science.* **2005**, *308*, 844–847.
[3] S. Park, J. M. Vohs, R. J. Gorte, *Nature.* **2000**, *404*, 265–267.
[4] S. M. Haile, *Acta Mater.* **2003**, *51*, 5981–6000.
[5] S. Chu, A. Majumdar, *Nature.* **2012**, *488*, 294–303.
[6] E. Fabbri, L. Bi, D. Pergolesi, E. Traversa, *Adv. Mater.* **2012**, *24*, 195–208.
[7] E. Fabbri, A. Depifanio, E. Dibartolomeo, S. Licoccia, E. Traversa, *Solid State Ionics.* **2008**, *179*, 558–564.
[8] L. Yang, S. Wang, K. Blinn, M. Liu, Z. Liu, Z. Cheng, M. Liu, *Science.* **2009**, *326*, 126–129.
[9] Y. Meng, J. Gao, H. Huang, M. Zou, J. Duffy, J. Tong, K. S. Brinkman, *J. Power Sources.* **2019**, *439*, 227093.
[10] C. Duan, R. J. Kee, H. Zhu, C. Karakaya, Y. Chen, S. Ricote, A. Jarry, E. J. Crumlin, D. Hook, R. Braun, N. Sullivan, R. O'Hayre, *Nature.* **2018**, *557*, 217–222.
[11] D. Medvedev, A. Murashkina, E. Pikalova, A. Demin, A. Podias, P. Tsiakaras, *Prog. Mater. Sci.* **2014**, *60*, 72–129.
[12] N. Kochetova, I. Animitsa, D. Medvedev, A. Demin, P. Tsiakaras, *RSC Adv.* **2016**, *6*, 73222–73268.
[13] D. Han, N. Hatada, T. Uda, *J. Electrochem. Soc.* **2016**, *163*, F470–F476.
[14] R. Slade, *Solid State Ionics.* **1995**, *82*, 135–141.
[15] D. Han, K. Shinoda, S. Sato, M. Majima, T. Uda, *J. Mater. Chem. A.* **2015**, *3*, 1243–1250.
[16] S. Wang, J. Shen, Z. Zhu, Z. Wang, Y. Cao, X. Guan, Y. Wang, Z. Wei, M. Chen, *J. Power Sources.* **2018**, *387*, 24–32.
[17] N. Kitamura, J. Akola, S. Kohara, K. Fujimoto, Y. Idemoto, *J. Phys. Chem. C.* **2014**, *118*, 18846–18852.
[18] J. Tong, D. Clark, M. Hoban, R. O'Hayre, *Solid State Ionics.* **2010**, *181*, 496–503.
[19] L. Bi, E. H. Da'as, S. P. Shafi, *Electrochem. Commun.* **2017**, *80*, 20–23.
[20] J. Zhu, G. Liu, Z. Liu, Z. Chu, W. Jin, N. Xu, *Adv. Mater.* **2016**, *28*, 3511–3515.
[21] Z. Zhang, Y. Zhu, Y. Zhong, W. Zhou, Z. Shao, *Adv. Energy Mater.* **2017**, *7*, 1700242.
[22] L. Chen, L. Liu, J. Xue, L. Zhuang, H. Wang, *J. Membr. Sci.* **2019**, *573*, 117–125.
[23] N. A. Tarasova, I.E. Animitsa, *Russ J. Electrochem. Soc.* **2013**, *49*, 698–703.
[24] F. Su, C. Xia, R. Peng, *J. Eur. Ceram. Soc.* **2015**, *35*, 3553–3558.
[25] Á. Triviño-Peláez, D. Pérez-Coll, G. C. Mather, *Acta Mater.* **2019**, *167*, 12–22.
[26] A. Løken, R. Haugsrud, T. S. Bjørheim, *Phys. Chem. Chem. Phys.* **2016**, *18*, 31296–31303.
[27] J. Niu, J. Deng, W. Liu, L. Zhang, G. Wang, H. Dai, H. He, X. Zi, *Catal.* **2007**, *126*, 420–429.
[28] W. Kohn, L. J. Sham, *Phys. Rev.* **1965**, *140*, A1133–A1138.
[29] G. Kresse, J. Furthmüller, *Comput. Mater. Sci.* **1996**, *6*, 15–50.
[30] G. Kresse, J. Furthmüller, *Phys. Rev. B.* **1996**, *54*, 11169–11186.
[31] J. P. Perdew, K. Burke, M. Ernzerhof, *Phys. Rev. Lett.* **1996**, *77*, 3865–3868.
[32] A. Otero-de-la-Roza, V. Luaña, *Comput. Phys. Commun.* **2011**, *182*, 1708–1720.

Manuscript received: January 28, 2020
Revised manuscript received: March 22, 2020